^{31}P Chemical Shifts in Ru(II) Phosphine Complexes. A Computational Study of the Influence of the Coordination Sphere

Christophe Raynaud,[a*] Eliott Norbert-Agaisse,[a] Brian R. James,[b*] Odile Eisenstein,[a,c*]

a) ICGM, Université de Montpellier, CNRS, ENSCM, Montpellier, 34095 France
b) Department of Chemistry, University of Vancouver, Vancouver, BC Canada V6T 1Z1 Canada
c) Department of Chemistry and Hylleraas Centre for Quantum Molecular Sciences, University of Oslo, Oslo 0315, Norway

Dedicated to Professor Pierre Dixneuf on the occasion of his 80th birthday

ABSTRACT:

NMR chemical shift has been the most versatile marker of chemical structures, by reflecting global and local electronic structures, and is very sensitive to any change within the chemical species. In this work, a set of Ru(II) complexes with the same five ligands and a variable 6th ligand L (none, H_2O, H_2S, CH_3SH, H_2, N_2, N_2O, NO^+, C=CHPh, and CO) is studied, using as the NMR reporter, the phosphorus P_A of a coordinated bidentate P_A–N ligand (P_A–N = *o*-diphenylphosphino-*N*,*N*′-dimethylaniline). The chemical shift of P_A in $RuCl_2(P_A–N)(PR_3)(L)$ (R = phenyl, *p*-tolyl or *p*-FC_6H_4) was shown to increase as the Ru–P_A bond distance decreases, an observation that was not rationalized. This work, using density functional theory (DFT) calculations, reproduces reasonably well the observed ^{31}P chemical shifts for these complexes, and the correlation between the shifts and the Ru–P_A bond distance as L varies. An interpretation of this correlation is proposed using a Natural Chemical Shift (NCS) analysis based on the Natural Bonding Orbital (NBO) method. This analysis of the principal components of the chemical shift tensors shows how the σ-donating properties of L have a particularly high influence on the phosphine chemical shifts.

INTRODUCTION

One of our groups first reported in 1993 on the square pyramidal complexes *trans*-$RuCl_2(P–N)(PR_3)$ (R = Ph, *p*-tolyl; P–N = *o*-diphenylphosphino-*N*,*N*′-dimethylaniline), and their ability to bind H_2 and N_2 to form, as final products, the six-coordinate *cis*-$RuCl_2(P–N)(PR_3)L$ (L = H_2, N_2) complexes.[1] Subsequently, the other relatively small molecules H_2S,[2,3] N_2O,[4] thiols,[5] CO,[6] NH_3,[6] and HC≡CPh, which is converted to coordinated C=CHPh,[7] reacted similarly to form related six-coordinate complexes, in which the chloride ligands are either *cis* or *trans*. Scheme 1 shows the *cis* and *trans* products for these

systems, although the L = H_2O and alcohol species were made via reactions with $RuCl_2(P–N)(PR_3)$ that was formed *in situ* from $RuCl_3(PR_3)_3$ complexes;[8] the most recent report describes a corresponding cationic *cis*-NO^+ species that was formed by reaction of *fac*-$RuCl_3(NO)(P–N)$ with PPh_3.[9] The two

Scheme 1. Schematic reactivity of *trans*-$RuCl_2(P_A–N)(PR_3)$ toward small molecules (L) to form isomeric six-coordinate complexes. *Note*: the *cis*-C=CHPh complex is formed by addition of HC≡CPh to the five-coordinate complex, and the NO^+ complex by reaction of PPh_3 with *fac*-$RuCl_3(NO)(P–N)$

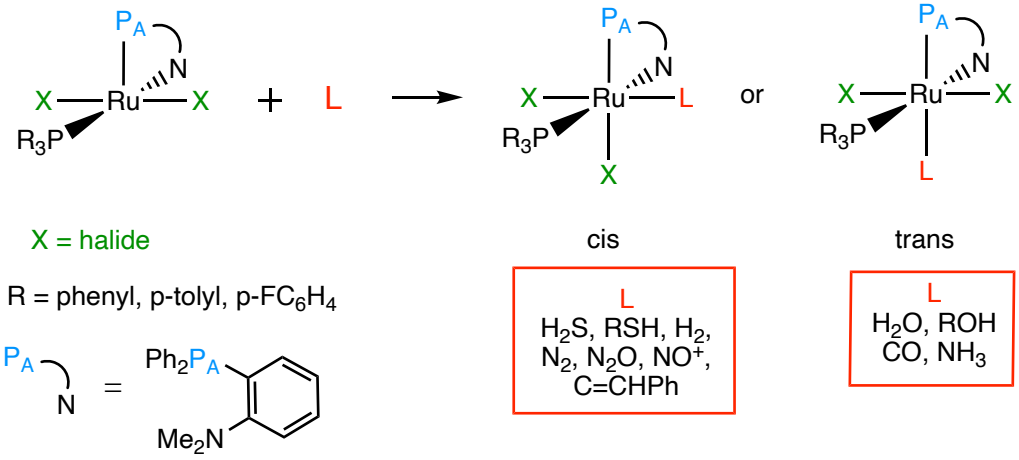

P-atoms in the complexes are labelled P_A and P (Scheme 1), as in the associated $^{31}P\{^1H\}$-NMR spectra, which show the expected doublet of doublets pattern. Crystals suitable for X-ray studies have been grown for many complexes, and an empirical inverse correlation between the $^{31}P_A$ chemical shift and the Ru–P_A bond length has been established over the respective ranges of about 30–80 ppm and 2.39–2.17 Å (Figure 1).[9] Of note, the complexes with different X groups (Cl or Br) and phosphines (PPh_3, P(*p*-tolyl)$_3$), or P(p-FC_6H_4) are present on this correlation line. Analogous trends exist for a more diverse range of Ru^{II}-complexes containing PPh_3[10] and $Ph_2P(CH_2)_4PPh_2$ ligands,[11,12] with the slopes and intercepts of all three plots being remarkably similar, about -3.0 x 10^{-3} Å ppm^{-1}, and ~2.43 Å, respectively. That the vinylidene complex *cis*-$RuCl_2(P_A–N)(PPh_3)(C=CHPh)$ had one of the longest Ru–P_A bonds within all the complexes was rationalized in terms of decreased Ru to P_A π-back-bonding because of competition with such bonding in the Ru=C moiety and, consistent with this, the shortest Ru–P_A bond is seen for the five-coordinate species $RuCl_2(P_A–N)[P(p\text{-tolyl})_3]$[1] (no solid-state structure was obtained for the corresponding PPh_3 complex), where maximum Ru to P_A π-back-bonding is likely be available.[7] The question of why the shortest bond results in a higher chemical shift remained unanswered. Indirect evidence for such 'π-back-bonding' effects, based on solid-state NMR studies[13,14] and theoretical work[15] on phosphoryl-containing compounds suggests that the degree of π-bonding

between P- and O-atoms is a key factor in governing the ^{31}P chemical shift tensors and P–O bond lengths. Thus, a DFT study on the $RuCl_2(P_A–N)(PR_3)L$ complexes seemed highly appropriate to help quantify details of the observed, inverse NMR/structural plot of Figure 1, and this led to the collaborative research described in this current paper. A theoretical study by Bühl's group[16] that derived a correlation between experimental or computed Rh–P bond lengths and computed ^{103}Rh chemical shifts for a series of Rh phosphine-containing complexes also encouraged us to venture into this area; of note, an increasing Rh–P bond length corresponded to an increase in the ^{103}Rh chemical shift, which is opposite to the correlation between the ^{31}P chemical shift and the Ru–P distance seen in Figure 1.

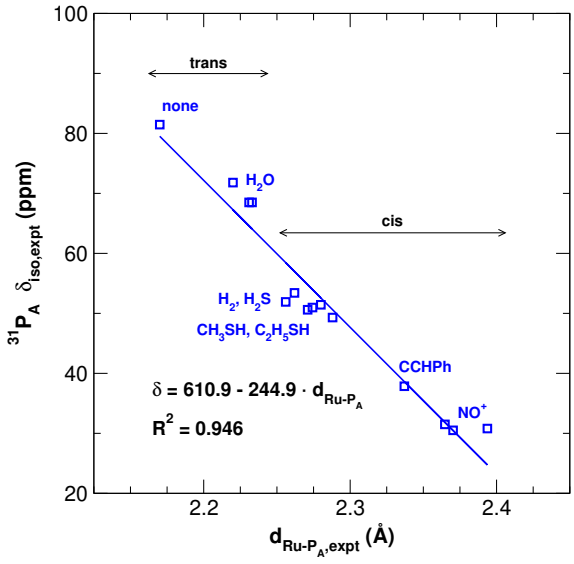

Figure 1. Plot of $^{31}P_A\{^1H\}$ experimental data *vs.* experimental Ru–P_A bond length (Å) for $RuCl_2(P_A–N)[P(p\text{-tolyl})_3]$ and the $RuX_2(P_A–N)(PR_3)L$ complexes, where X = Cl or Br, and R = Ph, *p*-tolyl or *p*-FC_6H_4 ; L is shown in Scheme 1; various crystalline forms are included when occurring; none is $RuCl_2(P_A–N)[P(p\text{-tolyl})_3]$.

COMPUTATIONAL DETAILS

All geometry optimizations were performed on the full molecules (neutral or charged) considered in vacuum with the Gaussian 09 package[17] at the PBE0-D3BJ level.[18,19] Ru was represented by relativistic effective core potential (RECP) from the Stuttgart group and the associated basis set.[20] The remaining atoms (H, C, N, O, Cl, Br, and P) were represented by a triple-ζ pcseg-2 basis set.[21] The analytically calculated harmonic frequencies were used to evaluate the zero-point energies (ZPE), the enthalpies and the Gibbs energies of all species at p = 1 atm and a temperature of 298.15 K. The coordinates of all optimized structures and associated energies are given in the Supporting Information, SI.

Calculations of NMR shieldings, σ, and related chemical shifts, δ, (eq 1, see below for σ^{ref}), were performed within the gauge-including atomic orbital (GIAO) framework using ADF 2016[22] with

the PBE0 functional on the full complexes in vacuum. Ru, P, and all atoms directly bonded to the metal and the P of interest were represented by Slater-type basis sets of triple-ζ quality (TZ2P), the remaining atoms being represented by a double-ζ quality Slater-type basis sets (DZP). Relativistic effects were treated by the 2-component zeroth order regular approximation (ZORA) including the spin-orbit contribution.[23] The results were found to improve with the inclusion of the spin-orbit contribution even if its magnitude is globally small (larger for the five-coordinate than the six-coordinate complexes).[24] The analysis of the electron density and scalar-relativistic natural localized orbitals was carried out with the NBO 6.0 program.[25] Calculated NMR shielding tensors were analyzed on the basis of the scalar-relativistic natural localized molecular orbitals (NLMOs).[26] To allow comparison between the species, all complexes were described with a consistent Lewis structure, involving three facial bonds: Ru–P_A. Ru–N, and Ru–P. It was verified that this Lewis structure represents properly the computed electron density for all complexes.

$$\delta = \frac{\sigma^{ref} - \sigma}{1 - \sigma^{ref}} \approx \sigma^{ref} - \sigma \qquad (1)$$

Literature has shown that calculations of the ^{31}P NMR shieldings, and thus of the chemical shifts, are challenging, since their values cover a range of 2000 ppm; a 10% accuracy in the calculation was recently still considered as "excellent".[27] Even the shielding in the simplest PH_3 is challenging to calculate.[28-30] The value of 328.35 ppm was first proposed for the shielding of the experimental compound used as reference, *i.e.* 85% aqueous H_3PO_4, [a_{85}-H_3PO_4].[31] Recently a revised value of 351.6 ppm was recommended.[32] This latter value was considered in this work. Of note, the value of the shielding for the reference is only important for comparing the calculated to the experimental chemical shifts and not for the trends, which are the main focus of this study. Also of note, the NMR measurements were carried out either in $CDCl_3$ or CD_2Cl_2 with very little impact on the NMR data as illustrated for $RuCl_2(P_A–N)[P(p\text{-tolyl})_3]$, where the P_A chemical shifts are 81.42 and 81.46 in CD_2Cl_2 and $CDCl_3$, respectively.[1, 8]

RESULTS

Structural Features of $RuCl_2(P_A–N)(PR_3)L$. The coordinates and a 3D representation of the optimized structures of all complexes are provided in the SI. For all ligands except L = CO, the six-coordinate complex of calculated lowest energy corresponds to the observed isomer, implying their thermodynamic preference; this is compatible with the synthetic method of the $RuCl_2(P_A–N)(PR_3)L$ complexes; *i.e.* by addition of L to the five-coordinate $RuCl_2(P_A–N)PR_3$, in which the empty coordination site is trans to P_A, or via ligand exchange within Ru precursors in solution. Of note, HC≡CPh, is converted to coordinated C=CHPh,[7] and the NO^+ complex is synthesized via a different route.[9] In contrast, the CO complex, *trans*-$RuCl_2(P_A–N)(PR_3)(CO)$, is formed, by an irreversible

reaction of CO to the powdered, five–coordinate *trans*-$RuCl_2(P_A–N)(PR_3)$; calculations show that the *cis* isomer is energetically preferred by $\Delta H = 9.6$ kcal mol^{-1}, (Table 1) suggesting that the *trans* isomer is a kinetic product.[33]

Table 1. Relative enthalpies (ΔH) and Gibbs energies (ΔG) in kcal mol^{-1} for the *cis* and *trans* isomers of $RuCl_2(P_A–N)(PR_3)L$; experimental and calculated $^{31}P_A$ NMR chemical shifts in ppm using the calculated value of 351.6 ppm for the isotropic shielding of the reference, [32] and the experimental and calculated $Ru–P_A$ distances in Å

#	L	isomer	$R(PR_3)$	ΔH	ΔG	$^{31}P\ \delta_{exp}$	$^{31}P\ \delta_{calc}$	$Ru–P_{A\ expt}$	$Ru–P_{A\ calc}$
1	none	*trans*	*p*-tolyl	-	-	81.5[a]	113.8	2.170(1)[1]	2.154
2	$CHCl_3$	*trans*	*p*-tolyl	-9.7	-10.5		87.4		2.194
3	$CHCl_3$	*cis*	*p*-tolyl	0.0	0.0		68.6		2.259
4	H_2O	*trans*	phenyl	-8.0	-8.1	68.5[a]	77.5	2.2305(14)[8]	2.203
5	H_2O	*cis*	phenyl	0.0	0.0		76.5		2.219
6	CH_3SH	*trans*	phenyl	4.3	4.5		47.7		2.280
7	CH_3SH	*cis*	phenyl	0.0	0.0	51.4[a]	60.3	2.2802(8)[5]	2.248
8	H_2S	*trans*	phenyl	4.1	3.4		50.8		2.273
9	H_2S	*cis*	phenyl	0.0	0.0	50.6[a]	55.3	2.2712(6)[5]	2.253
10	H_2S	*trans*	*p*-tolyl	2.2	1.1		51.8		2.280
11	H_2S	*cis*	*p*-tolyl	0.0	0.0	51.9[a]	55.7	2.2560(4)[2,]	2.252
12	N_2O	*trans*	phenyl	8.1	7.1		68.6		2.255
13	N_2O	*cis*	phenyl	0.0	0.0	49.1[b]	60.7	NA	2.249
14	N_2	*trans*	phenyl	8.5	10.7		58.8		2.305
15	N_2	*cis*	phenyl	0.0	0.0	47.2[b]	57.5	NA	2.263
16	H_2	*trans*	phenyl	4.9	6.9		52.1		2.273
17	H_2	*cis*	phenyl	0.0	0.0	49.3[a]	54.8	2.2884(7)[3]	2.252
18	NO^+	*trans*	phenyl	13.0	12.7		43.5		2.460
19	NO^+	*cis*	phenyl	0.0	0.0	30.9[c]	34.3	2.3937(10)[9]	2.344
20	C=CHPh	*trans*	phenyl	11.7	11.0		-2.5		2.515
21	C=CHPh	*cis*	phenyl	0.0	0.0	37.9[d]	25.2	2.337(2)[7]	2.304
22	CO	*trans*	phenyl	9.6	10.2	13.0[e]	6.9	NA	2.432
23	CO	*cis*	phenyl	0.0	0.0		39.0		2.272

The solvent used for recording the $^{31}P\{^1H\}$ chemical shift is listed with the associated reference. a) $CDCl_3$,[8] b) CD_2Cl_2,[4] c) CH_2Cl_2,[9] d) $CDCl_3$,[7] and e) $CDCl_3$.[6] NA not available.

The isomeric preference for the thermodynamically preferred complexes can be rationalized considering the σ-donating and π-accepting properties of L.[34,35] Thus, the vinylidene group which is both a strong σ-donor and a single face π-acceptor prefers to be *trans* to one of the two chlorides than to P_A (see Scheme 1 for labeling) by 11 kcal mol^{-1}, hence the preference for the *cis* isomer. Indeed, a chloride ligand has a weak trans influence and also enhances the back-donation of one Ru lone-pair into the empty p orbital of vinylidene Cα via 4e d_π-p_π interaction.[36] The larger donation (L → Ru) and backdonation (Ru → p($C\alpha_{C=CHPh}$)) in the *cis*- over the *trans*- isomer are confirmed by the NBO analysis (Table S18 in the SI). Similar effects account for the preference for the *cis* over the *trans* isomer for L = NO^+, N_2, N_2O (bonded via N as shown in the SI), and H_2 by ΔG of 12.7, 10.7, 7.1, and 6.9 kcal mol^{-1}, respectively. Thus, all L ligands with π-accepting ability[37] coordinate *cis* to P_A with the notable exception of CO, whose complex is not under thermodynamic control.

When the L ligand is a modest σ-donor and has no π-accepting ability, the energy preference for the *cis* isomer is either small, or the *trans* isomer is slightly more stable. The five-coordinate $RuCl_2(P_A–N)(PR_3)$ has the empty coordination site *trans* to P_A as illustrated in Scheme 1.[1] If L interacts weakly with the Ru complex, the structural preference of the five-coordinate species determines that of the six-coordinate $RuCl_2(P_A–N)(PR_3)L$; this accounts for the preference of *trans*-$RuCl_2(P_A–N)(PR_3)(H_2O)$. The marginally stronger ligand H_2S induces a slightly larger perturbation to the five-coordinate species, resulting in almost isoenergetic *cis*- and *trans*- isomers; this is illustrated by the preference for the *cis*-isomer by 3.4 or 1.1 kcal mol^{-1} when the monodentate phosphine is PPh_3 or P(*p*-tolyl)$_3$, respectively. Under kinetic control, the preference for the *trans* isomer in the case of the CO ligand results from a direct addition to the vacant site of the five-coordinate Ru complex.

There is a general fair agreement between calculated and observed bond lengths even if the calculated bond distances are generally slightly shorter than the distances given by X-ray diffraction values. (Tables S4 and S6-S9 in the SI). This is likely due to intermolecular interactions present in the crystal that are not included in the calculations. Geometry optimizations carried out for a single molecule in vacuum, with a computational method that includes the dispersion corrections have been shown to give bond distances that are too short.[38] A noticeable discrepancy is obtained for L = NO^+. For this ligand, the solid-state structures of $RuCl_2(P_A–N)(PR_3)(NO)^+$ reveal that Ru-N(nitrosyl) bond distance depends on the nature of the monodentate PR_3, as shown by values of 1.794(5), 1.870(5), and 1.738(3) Å, for P(*p*-tolyl)$_3$, PPh_3, and P(p-FC_6H_4)$_3$, respectively (Table S8 in the SI).[9] Geometry optimization carried out with PPh_3 does not reproduce the observed, long Ru–N(nitrosyl) distance. However, since the $^{31}P_A$ chemical shifts (and other spectroscopic data) are similar for the three phosphine ligands,[9] the Ru-N(nitrosyl) distance is probably similar in solution for the three NO^+ complexes.

Isotropic $^{31}P_A$ Chemical Shifts. The $^{31}P_A$ chemical shifts, δ^{P_A}, of $RuCl_2(P_A–N)(PR_3)L$, were calculated for the *cis*- and *trans*-isomers, regardless of the structural preferences, in order to determine

the impact of the coordination site of L on the chemical shift of P_A, (Table 1 and Figure 2). The ^{31}P chemical shifts of the monodentate phosphine were also calculated, they vary little with L and are less informative, the corresponding data are reported in the SI and are not discussed in detail (Table S3). Good agreement is obtained between experimental and calculated chemical shifts for P_A, with the exception of the five-coordinate $RuCl_2(P_A–N)[P(p\text{-tolyl})_3]$ complex (#1) for which the observed δ^{P_A} in $CDCl_3$ is 81.5 ppm[1] and the calculated value is 113.8 ppm. Since the difference between experimental and calculated values is < 15 ppm for all other complexes, this larger discrepancy of ~ 32 ppm may not be due to the computational method. This five-coordinate complex, in the absence of an agostic interaction (not present in the solid state or in the computed optimized structure) likely binds a $CDCl_3$ ligand and forms six-coordinate $RuCl_2(P_A–N)(PR_3)(CDCl_3)$ in solution. Optimization of this complex gave a *trans* η^1–Cl_3CD complex (#2) with a Ru···Cl distance of 2.79 Å and also a less stable *cis* isomer (#3); further, for this complex #2, the calculated δ^{P_A} of 87.4 ppm is only 6 ppm away from the experimental value. This is considered a good indication that the NMR data for this five-coordinate complex, in fact, refer to a solvated species with a weakly coordinated $CDCl_3$.

The agreement between calculated and experimental chemical shifts for P_A in this set of complexes is good as illustrated by an R^2 of 0.964, excluding #1 from the correlation (Figure 2). Including dynamic effects and explicit solvation of the molecular species, in addition to representation of the relativistic effects with 4-components calculations, would be required to achieve high accuracy as illustrated recently for *trans*-$PtCl_2(NHMe_2)(PPh_3)$ in water.[39] In fact, the lack of consideration of the diversity of possible conformations could account for the 13 ppm difference between the observed and calculated chemical shifts in the case of L = C=CHPh (#21). For probably related dynamic effects, the agreement between calculated and experimental ^{31}P chemical shifts was found to be significantly lower for the monodentate phosphine than for P_A of the bidentate P_A–N ligand (Table S3 in the SI vs Table 1).

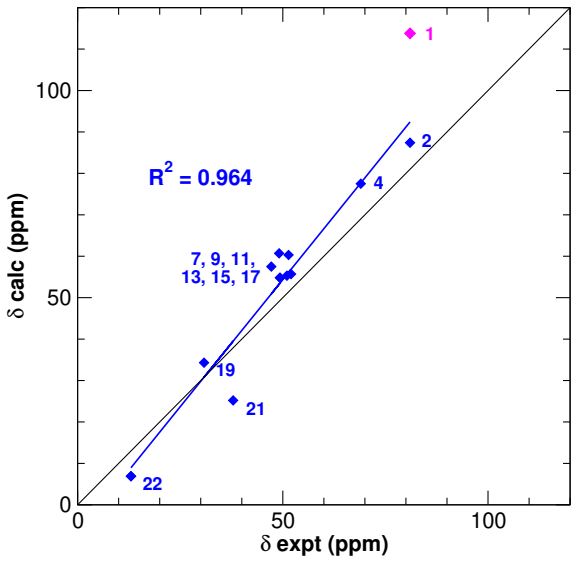

Figure 2. Calculated *vs.* experimental $^{31}P_A$ chemical shifts for $RuCl_2(P_A–N)(PR_3)L$. See Table 1 for labelling of the complexes. The reference value for calculating ^{31}P chemical shifts is 351.6 ppm.[32]

Figure 1 presented the linear relationship between experimental $^{31}P_A$ chemical shifts in solution and Ru–P_A bond distances determined in the solid state. A similar relationship holds for computed values and even when all isomers (observed and not observed) are included, as shown in Figure 3 where blue squares and red triangles refer to the observed and non-observed species, respectively. However, the correlation is better when considering the observed isomers only (blue line $R^2 = 0.960$) than all isomers (black line $R^2 = 0.857$). Three complexes are far from the correlation line, like $RuCl_2(P_A–N)(P(p\text{-tolyl})_3)$ (#1), *trans*-$RuCl_2(P_A–N)(PPh_3)(NO)^+$ (#18) and also *cis*-$RuCl_2(P_A–N)(PPh_3)(C{=}CHPh)$ (#21). Thus, the correlation between δ^{P_A} and Ru–P_A bond distances appears good, but the presence of exceptions suggests care in a more general application.

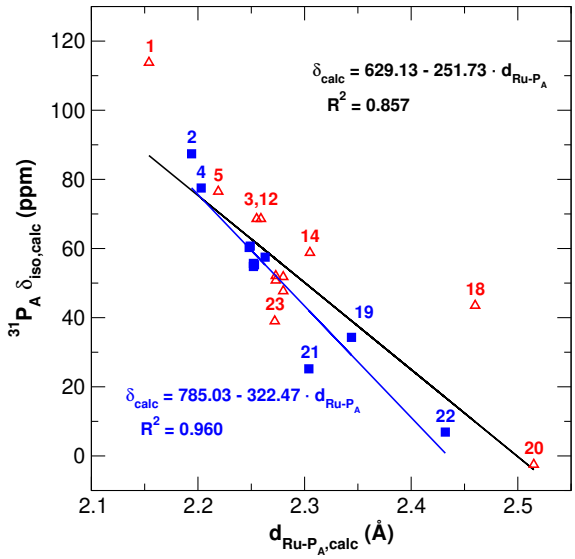

Figure 3. Calculated chemical shifts δ^{P_A} (ppm) *vs*. calculated Ru–P_A distances (Å). The blue full squares and red empty triangles correspond to observed and non-observed isomers, respectively. For labelling of complexes, see Table 1.

As expected, the calculated chemical shifts differ for the *cis* and *trans* isomers, but the difference between these values depends on L. With the weakly bonded ligands H_2O, H_2S, CH_3SH, N_2O, N_2 and H_2 the calculated δ^{P_A} are similar for the two isomers with no clear trend for which isomer has the higher chemical shift. It is thus rather difficult to use the calculated chemical shift to assign the *cis* or *trans* nature of the isomer by comparison with the experimental shift. The situation is better with more strongly bonded ligands such as NO^+, C=CHPh and CO (#18-23). This confirms the *cis* nature for the experimental NO^+ and C=CHPh complexes and *trans* nature for the CO complex. Similarly, the

calculations indicate clearly that the empty coordination site (or the weakly interacting $CDCl_3$ solvent) is *trans* to P_A ((#1-2).

DISCUSSION

Charge transfer from L to $RuCl_2(P_A–N)(PR_3)$ To understand how L influences the chemical shifts of P_A, one needs first to analyze how L tunes the electronic structure of $RuCl_2(P_A–N)(PR_3)$ around P_A. A meaningful way to obtain this information is to consider that the six-coordinate complex is formed by the union of $RuCl_2(P_A–N)(PR_3)$ and L, and study this interaction using the NBO method.[25] In an NBO vision, the bonding is described by donor/acceptor interactions; the key one is delocalization of the electron density on L, usually localized in a lone-pair according to the NBO analysis, into vacant antibonding σ* type NBOs (antibonds) between Ru and the ligands of the five-coordinate fragment.[25,40] This delocalization leads to charge transfer from L to the vacant σ* NBOs; due to the absence of symmetry of the complexes, charge transfer occurs also in antibonds that are *cis* and *trans* to L. As expected, the charge transfer increases with the σ-donor strength of L but is always significantly less than 2e. Therefore, the partial occupancy of a σ* NBO antibond leads to lengthening but not cleavage of the Ru-ligand bond. In term of molecular orbitals (which can always be expressed as linear combinations of NBOs), partial occupancy of a σ* NBO is associated with a raise in energy of all vacant (canonical) molecular orbitals that have contributions from this σ* NBO.

Here, focus on the $Ru–P_A$ bond is needed, and thus the partial occupancy of the $\sigma(Ru–P_A)$ and $\sigma^*(Ru–P_A)$ NBOs were calculated (Table S17 in the SI). The partial occupancy of $\sigma(Ru–P_A)$ NBO is around 1.89e for all L. In contrast, the partial occupancy of $\sigma^*(Ru–P_A)$, $n\sigma^*(Ru–P_A)$, is very sensitive to the nature of L. This partial occupancy, which is the smallest (0.15e) for the five-coordinate complex #1, increases in a modest manner (0.2 to 0.4e) for weak σ-donors like H_2O, H_2S, CH_3SH, and N_2O, (#4-13) and becomes significant (0.5 to 0.65e) for strong σ-donor L like NO^+, C=CHPh, and CO (#18-23). Increasing $n\sigma^*(Ru–P_A)$ lengthens the $Ru–P_A$ bond (Figure S6 in the SI) although the correlation is modest ($R^2 = 0.652$) because several additional donor/acceptor σ-and π-interactions contribute to the global interaction of the two fragments.

Correlation between Isotropic Shielding at P_A and Electronic Properties at P_A. The following uses both the chemical shift (δ^{P_A}) and the shielding (σ^{P_A}) terms. As currently recognized,[41-43] the NMR shielding of P_A is not expected to correlate well with the atomic charge on the active nucleus. This is the case also for the complexes in the present work (Figure S7 in the SI). In attempts at understanding the observed correlation between the $\delta^{P_A}/\sigma^{P_A}$ and the $Ru–P_A$ bond distance, a search was made for an electronic property that could correlate with these factors, and a remarkably good correlation ($R^2 = 0.912$, Figure 4) was found between the calculated shielding at P_A, σ^{P_A}, and the electron

occupancy of the σ*(Ru–P_A) NBO, nσ*(Ru–P_A), defined in the previous section. Thus, the isotropic shielding and the Ru–P_A bond distance both increase as nσ*(Ru–P_A) increases, *i.e.* as more electron density is transferred to the σ*(Ru–P_A) NBO. This naturally establishes a correlation between $\delta^{P_A}/\sigma^{P_A}$ and the Ru–P_A bond distance, as observed experimentally. While this is gratifying phenomenologically, an understanding is developed in the following section.

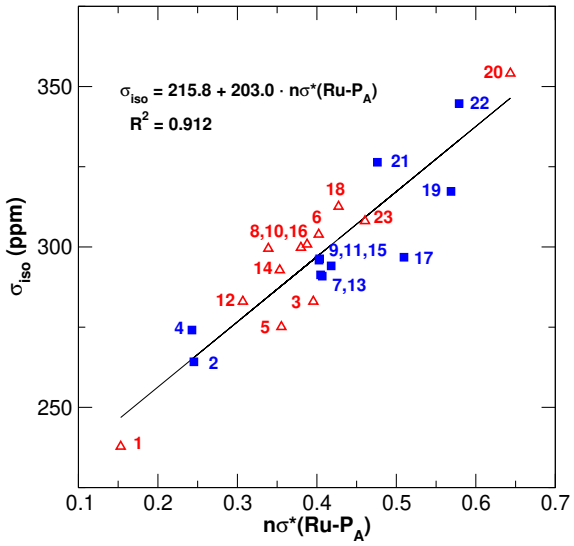

Figure 4. Isotropic shielding *vs.* the occupancy, nσ*(Ru–P_A), of the σ*(Ru–P_A) NBO.

The tuning of the P_A Chemical Shift (Shielding) Tensor by L. In recent literature, there has been an increasing number of studies focused on the relationship between the chemical shifts/shieldings and bonding features of the selected nucleus and the interested reader is referred to selected articles and reviews.[26,44-48] These studies have been extremely useful in getting deeper insight on the bonding properties around the studied atom, with possible extrapolation to other properties such as reactivity.[49-55] The flourish of recent studies for a high diversity of atoms is a clear indication that chemists wish to learn more NMR information. The literature is abundant for main group elements and only selected references are given. Carbon[50-57] and silicon[58] were considerably studied. More recently aluminium,[59] yttrium,[60] oxygen,[61] selenium,[62] and tellurium[63] were also considered. Phosphorus has been studied in systems with and without a transition metal.[64-68] For instance, the nature of the carbon-phosphorus double and triple bonds was interpreted by solid-state NMR.[64] The unusually high chemical shift of a metal-bound phosphido group was shown by calculations to be associated with a high paramagnetic term.[65] Solid-state NMR studies and analysis of the chemical shift tensor have been combined on a variety of phosphine-containing complexes using computational methods similar to the one used in the current work. [66-68]

The key information is the chemical shift anisotropy (CSA), which can be measured by solid-state NMR and calculated by quantum methods. It is represented by a second rank tensor whose components in the principal axes frame are δ_{11}, δ_{22}, δ_{33} ($\delta_{11} \geq \delta_{22} \geq \delta_{33}$); the isotropic chemical shift is the average of these three components (equation 2) and a similar quantity in terms of shieldings ($\sigma_{11} \leq \sigma_{22} \leq \sigma_{33}$) is used below. A measure of the anisotropy is represented by the span Ω -difference between δ_{11} and δ_{33}.

$$\delta_{iso} = \frac{1}{3}(\delta_{11} + \delta_{22} + \delta_{33}) \qquad (2)$$

For all complexes computed in this work, one of the principal axes of the shielding tensor is approximatively along the Ru–P_A direction and the other two are approximatively perpendicular to it. (Table S11, and Figures S3, S4, and S5 in the SI). Thus, although the complexes have no symmetry elements, the directions of the principal axes are characteristic of an octahedral type coordination as established for phosphine complexes of higher symmetry.[67] As a consequence of the absence of symmetry elements, the two principal axes that are perpendicular to the Ru–P_A "axial" direction do not have specific orientation relative to the four ligands in the "equatorial plane". Their orientations change with L and its *cis* or *trans* position relative to P_A. However, for essentially all complexes, the two axes perpendicular to the Ru–P_A direction are associated with the most deshielded components, *i.e.* σ_{11} and σ_{22}. Of note, however, for *cis* NO^+ (#19), and to a lesser extent *cis* C=CHPh (#21), the principal axes associated with the σ_{22} and σ_{33} components deviate from being perpendicular and parallel, respectively, to the Ru–P_A direction. Fortunately, these deviations do not impact significantly on the analysis.

In a nonrelativistic formalism, the shielding can be split into diamagnetic and paramagnetic (usually deshielding) contributions.[69] Within the GIAO framework, the calculations show that the diamagnetic contribution for P_A in all species of Table 1 is essentially constant and is also isotropic (Table S12 in the SI). Thus, the variation in chemical shifts as a function of L must be attributed to the paramagnetic contribution, which includes also the spin-orbit term in this work. This is nicely illustrated by the almost perfect correlation between σ_{iso} and σ^{p+so} with a slope of 0.995 and R^2 of 0.9997 (Figure 5 left and Table S12 in the SI). Analysis of the terms σ_{11}^{p+SO}, σ_{22}^{p+SO}, and σ_{33}^{p+SO}, which are the paramagnetic plus spin-orbit shieldings in the principal axis frame, is thus sufficient to explain the behavior of σ^{p+so}, and thus of σ_{iso}.

Calculations show that σ_{11}^{p+SO} and σ_{22}^{p+SO} vary significantly with L whereas σ_{33}^{p+SO} is more constant (Table S12, in the SI). Therefore, this latter term cannot be responsible for the variation of σ_{iso}. Further, the correlations between σ_{iso} and σ_{11}^{p+SO} or σ_{22}^{p+SO}, independently, are reasonable (R^2 of 0.930 and 0.884, respectively, Figure S1 in the SI). However, the slopes of these correlations are similar, suggesting equal contributions. Indeed, the correlation between σ_{iso} and $1/3(\sigma_{11}^{p+SO} + \sigma_{22}^{p+SO})$ with an

excellent R^2 of 0.9863 and a slope of 0.844 shows that the paramagnetic contributions of the two most deshielded terms to the averaged paramagnetic shielding σ^{p+so} quantitatively describe the changes of the isotropic shielding σ_{iso}. We now analyze the reasons for this behavior.

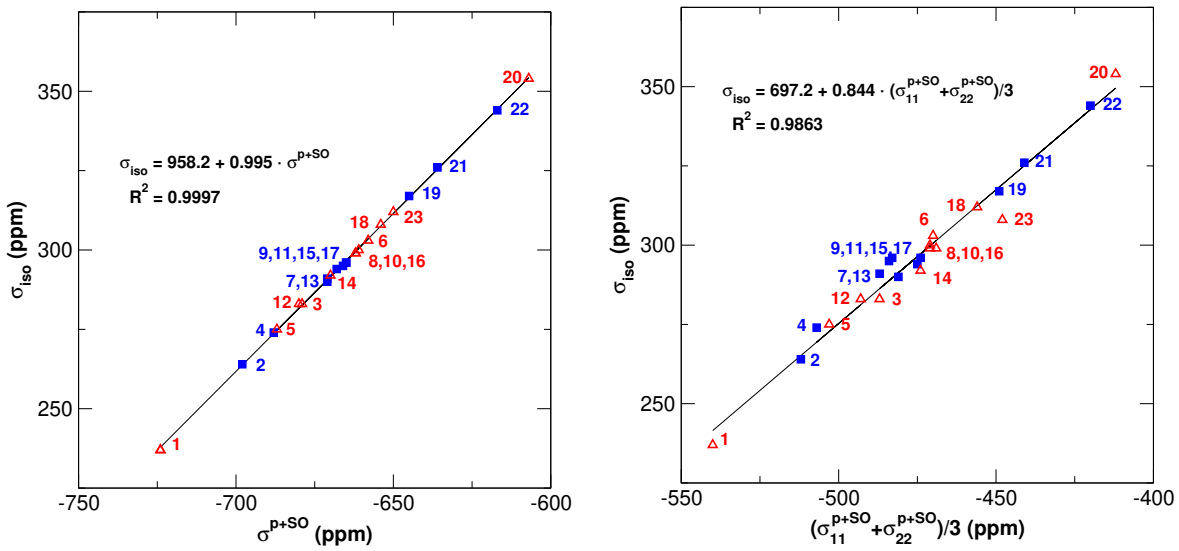

Figure 5. Isotropic shielding σ_{iso} *vs.* (left) σ^{p+so} and (right) $(\sigma_{11}^{p+SO} + \sigma_{22}^{p+SO})/3$.

An analysis of the shielding principal components σ_{11}, σ_{22} and σ_{33}, was performed in terms of molecular orbitals (MOs). To understand the origin of the contributions of the various MOs to the paramagnetic terms[70] a convenient approach is that of the 'orbital rotation model'.[56,71,72] Focus being on phosphorus, all MOs having contributions on the P_A–C and Ru–P_A bonds are of interest. The orbital rotation model is illustrated in Scheme 2 with selected contributions of the phosphorus orbitals to these bonds. For instance, the $3p_y$ orbital contributes to MOs having P_A–C bonding character. Applying the magnetic field along the x direction can be thought of as rotating the $3p_y$ orbital around the x axis by 90°, this yielding a rotated orbital aligned with the z axis. Thus, the *occupied* MOs with $3p_y$ orbital character overlap, after rotation, with an *empty* MO with σ*(Ru–P_A) character. This coupling results in a paramagnetic contribution at P_A associated with the x direction. An analogous development can be done with the P_A $3p_z$ orbital, which contributes to MOs having Ru–P_A bonding character. Applying the magnetic field along the x direction can be thought of as rotating the $3p_z$ orbital around the x axis, this yielding a rotated orbital along the y direction. The occupied MOs with $3p_z$ character overlap, after rotation, with an *empty* orbital that is antisymmetrical relative to the xz plane such as the schematic orbital shown on the right-hand side of Scheme 2. The corresponding coupling between these orbitals also yields a paramagnetic term associated with the x axis. The magnitude of the paramagnetic contributions increases with increasing overlap between the occupied and empty MOs and decreasing energy gap. Similar schemes apply to the magnetic field along the y direction (rotation around y). In

this case, the $3p_x$ and $3p_z$ orbitals of phosphorus contribute to a paramagnetic term associated with the y direction. Finally, the magnetic field along the z direction is associated with contributions from MOs with $3p_x$ and $3p_y$ characters and a resulting paramagnetic field associated with the z direction. The paramagnetic terms σ_{11} and σ_{22} are associated with the magnetic field along the x and y axes, while σ_{33} is associated with that along z axis. The contributions of the MOs were calculated for the three principal components. For all of them, a large number of small contributions is found, making interpretation of the results in term of bonding pattern challenging. Presenting the results in a more compact way is thus preferable. This is achieved with the localization procedure provided by the Natural Chemical Shift (NCS) analysis, implemented in the NBO method; this analysis describes the diamagnetic and paramagnetic contributions, notably in terms of lone-pairs and bonds. Comparison between complexes #1-23 is possible if a similar Lewis structure is selected for all systems. Therefore, the NCS analysis was carried out using the Lewis structure that was also used to calculate the occupancy of the $\sigma^*(Ru–P_A)$ NBO. This procedure reduces considerably the number of terms; four emerge: $P_A–C$ and $Ru–P_A$ bonds, the Ru lone-pairs and P_A core orbitals that contribute roughly in comparable amounts to the paramagnetic terms of σ_{11}, σ_{22} and σ_{33} (Tables S13-S15). Unfortunately, none of these four contributions correlate well with the full paramagnetic term of each principal component for all complexes #1-23. However, it is sufficient to consider the contributions of the $P_A–C$ and $Ru–P_A$ bonds to σ_{11} and σ_{22} to understand why the five-coordinate species and its solvated variant (#1-2), have the most deshielded P_A, and six-coordinate species with L = NO^+, C=CHPh and CO, (#18-23), have the most shielded P_A. In fact, the contributions of the $P_A–C$ bonds to the paramagnetic terms of σ_{11} and σ_{22} vary considerably, and alone determine the low shieldings for #1-2 and the high ones for #18-23. An opposite, but smaller, variation is found from the contribution of the $Ru–P_A$ bond; thus, this contribution moderates the very large change in shielding associated with the contribution from the $P_A–C$ bonds. Together, the sum of these two contributions account well qualitatively for the high and low chemical shifts of complexes #1-2 and #18-23, respectively. Nevertheless, these two terms, together, do not correlate well with the variation of the paramagnetic terms of σ_{11} and σ_{22} for the entire series, #1-23; additional contributions are needed. Since the contributions from the $P_A–C$ and $Ru–P_A$ bonds are needed to define the complexes with the lowest and highest P_A chemical shifts, they are worth exploring further.

As suggested by the NCS analysis, and illustrated in Scheme 2, the contribution of the $P_A–C$ term to the paramagnetic term along the x direction depends on the 'overlap' of the rotated P_A $3p_y$ orbital with the $\sigma^*(Ru–P_A)$ NBO. It also depends on the difference in energy between the MOs with $P_A–C$ and $\sigma^*(Ru–P_A)$ NBOs contributions. Qualitatively, the MOs with $P_A–C$ contributions are likely to be influenced little by the coordination at the ruthenium center. In contrast, the energies of empty MOs with $\sigma^*(Ru–P_A)$ NBO character are likely to be significantly influenced by this coordination and use of the partial occupancy $n\sigma^*(Ru–P_A)$ of the $\sigma^*(Ru–P_A)$ NBO is proposed to establish tendencies. Mentioned earlier was that empty MOs with $\sigma^*(Ru–P_A)$ NBO character are expected to be low in energy

when nσ*(Ru–P_A) is small. This is the case for #1-2 where nσ*(Ru–P_A) is < 0.25e (Table S17); this leads to large P_A–C bond deshielding paramagnetic contributions to σ_{11} and σ_{22}, for #1-2, as indeed calculated (Tables S13 and S14). Following the same analysis, there is much less deshielding contribution from the P_A–C bonds in the case of #18-23; for these systems, nσ*(Ru–P_A) is large (around 0.5-0.6e), and in fact the calculations give a shielding contribution. A related analysis can be done for the contribution of the σ(Ru–P_A) NBO to the paramagnetic terms of σ_{11} and σ_{22}. A schematic representation of an empty orbital, which can couple with the rotated σ(Ru–P_A) NBO, is shown on the right-hand side of Scheme 2 in the case of L = CO. Such an empty orbital is at low energy when L has π-accepting character. This accounts for a significant deshielding paramagnetic contribution originating from the Ru–P_A bond for ligands like NO^+, C=CHPh and CO (#18-23). Thus, the contributions from P_A–C and Ru–P_A bonds have opposite consequences on the shielding of P_A but the contribution from the P_A–C bonds varies more across the whole set #1-23, which results in P_A being the most deshielded in the complexes #1-2 and the least in the complexes #18-23. This also explains why nσ*(Ru–P_A) appears to be a good compact descriptor for the P_A chemical shift. In addition, nσ*(Ru–P_A) correlates well with the chemical shifts for the entire series #1-23, (Figure 4) which is probably due to additional, non-identified, small contributions.

The ^{31}P chemical shift is thus highly sensitive to the coordination sphere of the phosphine complex, but cannot be related to the donor/acceptor property of the phosphine acting as a response for a change of L. Analysis of the ^{31}P chemical shift is based on the occupied and empty orbital pattern of the whole complex, which is itself tuned by the coordinated ligands. However, informative is that a good correlation is shown to exist between the ^{31}P chemical shift and the occupancy of a σ*(Ru–P_A) NBO, nσ*(Ru–P_A), obtained from an NBO analysis of the complex considered as the union of $RuCl_2(P_A–N)(PR_3)$ and L. This suggests that the P_A chemical shift is more strongly influenced by the σ–metal-ligand field than by its donor/acceptor characteristics.

Scheme 2. Schematic representation of the rotated orbital model for a magnetic field along the x direction resulting into paramagnetic couplings. (Left) $3p_y$ orbital, contributing to the P_A–C bond, coupled with the σ*(Ru–P_A) NBO after 90° rotation around x axis; L is not specified. (Right) $3p_z$ orbital, contributing to the Ru–P_A bond, coupled with a schematic vacant orbital (L = CO) after rotation by 90° around the x axis

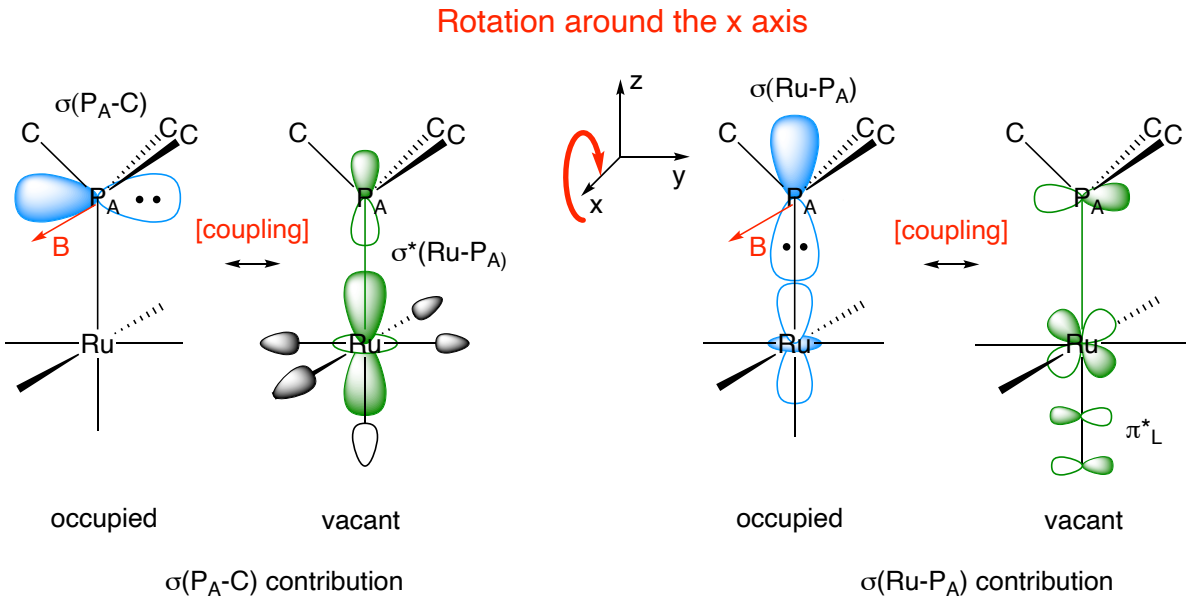

CONCLUSIONS

This computational study of $^{31}P_A$ NMR chemical shifts/shieldings in $RuCl_2(P_A–N)(PR_3)L$ complexes (L = none, H_2O, H_2S, CH_3SH, N_2O, H_2, N_2, NO^+, C=CHPh, and CO) provides an understanding of the dependence of δ^{P_A} on the nature and coordination site of L. The earlier experimental studies established a linear relationship between δ^{P_A} and the solid-state Ru–P_A bond distance, raising the question of why such a correlation exists. This correlation is reproduced with calculated values, where the number of systems is enlarged by considering primary and secondary isomeric forms of $RuCl_2(P_A–N)(PR_3)L$. The chemical shifts calculated with the 2-component ZORA method, including spin-orbit corrections, on the full models of $RuCl_2(P_A–N)(PR_3)L$, reproduce the observed chemical shifts well using the latest proposed value for the reference compound (351.6 ppm). The calculations also suggest that the NMR measurements have probed a $CDCl_3$ solvated $RuCl_2(P_A–N)[P(p\text{-tolyl})_3]$, even though there is no experimental evidence for this.

There is no relation between δ^{P_A} and the charge on this atom. In contrast, a good correlation exists between δ^{P_A} and the occupancy of the σ*(Ru–P_A) NBO, nσ*(Ru–P_A), calculated by an NBO analysis in which $RuCl_2(P_A–N)(PR_3)L$ is built from $RuCl_2(P_A–N)(PR_3)$ and L. In this correlation, increasing nσ*(Ru–P_A) decreases δ^{P_A} and thus, a weak electron donor L is associated with a small nσ*(Ru–P_A) and high δ^{P_A}. In contrast, a strong σ-electron donor L leads to a large nσ*(Ru–P_A) and low δ^{P_A}. This accounts also for the correlation between δ^{P_A} and the Ru–P_A bond distance since low nσ*(Ru–P_A) is associated with a shorter Ru–P_A bond distance.

To understand the correlation of δ^{P_A} with nσ*(Ru–P_A), an analysis of the shielding at P_A was conducted with the NCS analysis associated with the NBO method. The variation of δ^{P_A} is determined

by the paramagnetic term of the two most deshielded components (σ_{11} and σ_{22}) of the shielding tensor at P_A, both components being associated with the principal axes that are essentially perpendicular to the Ru–P_A direction. An analysis of σ_{11} and σ_{22} shows a deshielding contribution from the paramagnetic coupling of occupied orbitals having P_A–C bonding character with vacant ones having σ^*(Ru–P_A) character. Low occupancy of the σ^*(Ru–P_A) NBO increases the paramagnetic coupling and thus δ^{P_A}, which accounts for $RuCl_2$(P_A–N)[P(*p*-tolyl)$_3$] having the highest δ^{P_A}. Increasing the occupancy of σ^*(Ru–P_A) NBO, as a result of the charge transfer from L to the five-coordinate Ru fragment, lengthens the Ru–P_A bond and decreases the paramagnetic coupling. Thus, the high sensitivity of δ^{P_A} to L reflects mostly the σ-donating characteristics of this ligand and notably the availability of the empty orbitals with antibonding Ru–P_A character for involvement in paramagnetic coupling.

ASSOCIATED CONTENT

Supporting Information

The Supporting information is available free of charge at https://pubs.acs.org/doi/

Energetics, experimental and calculated structural information, experimental and calculated chemical shifts/shieldings for P_A and the monodentate phosphine. NBO analysis $RuCl_2$(P–N)(PPh_3)L viewed as the union of $RuCl_2$(P–N)(PPh_3) and L. Principal components σ_{11}, σ_{22} and σ_{33} for P_A. Orientation of the principal axes of the shielding tensors. Diamagnetic and paramagnetic contributions for σ_{11}, σ_{22} and σ_{33} for P_A. NCS analysis of σ_{11}, σ_{22} and σ_{33} principal components for P_A. NPA charges at P_A and Ru and the phosphorus of the monodentate phosphine. Electron occupancy of σ(Ru–P_A) and σ^*(Ru–P_A) NBOs. NBO analysis for the study of the *cis*/*trans* isomeric preference. Graphical representation of several correlations. Coordinates and 3D representation of all optimized complexes in the Supporting Information. Coordinates of all complexes as xyz file directly readable with Mercury.

AUTHOR INFORMATION

Corresponding Authors

*E-mail christophe.raynaud1@umontpellier.fr

*E-mail : odile.eisenstein@umontpellier.fr

*E-mail: brj@chem.ubc.ca

ORCID

Christophe Raynaud: 0000-0003-0979-2051

Brian James: 0000-0003-3541-7984

Odile Eisenstein: 0000-0001-5056-0311

NOTES

The authors declare no competing financial interest.

ACKNOWLEDGEMENTS

This work was initiated following a visit of OE to UBC with lectureship from the French Lecture series sponsored by the French Embassy in Canada. OE was partially supported by the Research Council of Norway through its Centre of Excellence Scheme Project (Hylleraas Centre, grant 262695) and the earlier Centre of Excellence project (CTCC (grant 179568/V30). The authors are grateful to Dr Heike Fliegl now at the Institute of Nanotechnology (INT), Karlsruhe Institute of Technology (KIT), who performed early test calculations when she was at the CTCC in Oslo and to Dr Michal Repisky from the Hylleraas centre at the Artic University of Norway for useful discussions. Presented calculations were carried out in Montpellier using the French national facilities (GenCI grant A0070810475).

REFERENCES

1. Mudalige, D. C.; Rettig, S. J.; James, B. R.; Cullen, W. R. Molecular-Hydrogen, -Nitrogen and Monohydride Derivatives of the Structurally Characterized Dichloro(o-diphenylphosphino-N,N-dimethylaniline) [tris(*p*-tolyl)phosphine]ruthenium(II) Complex. *J. C. S. Chem. Commun.* **1993**, 830-832.
2. Mudalige, D. C.; Ma, E. S.; Rettig, S. J.; James, B. R.; Cullen, W. R. Synthesis and X-ray Structure of an H_2S Complex $RuCl_2(P–N)(P(p\text{-tolyl})_3)(SH_2)$ (P–N = o-(Diphenylphosphino-N,N-dimethylaniline). *Inorg. Chem.* **1997**, *36*, 5426-5427.
3. Ma, E. S. F.; Mudalige, D. C.; Patrick, B. O.; James, B. R. Comparative Properties of coordinated H_2 and H_2S at a Ruthenium(II) Centre. *Dalton Trans.*, **2013**, *42*, 7614-7621.
4. Pamplin, C. B.; Ma, E. S. F.; Safari, N.; Rettig, S. J.; James, B. R. The Nitrous Oxide complex $RuCl_2(\eta^1\text{-}N_2O)(P–N)(PPh_3)$ (P–N= [o-(N,N-Dimethylamino)phenyl] diphenylphosphine); Low Temperature Conversion of N_2O to N_2 and O_2. *J. Am. Chem. Soc.* **2001**, *123*, 8596-8597.
5. Ma, E. S. F.; Rettig, S. J.; Patrick, B. O.; James, B. R. Ruthenium(II) Thiol and H_2S Complexes: Synthesis, Characterization and Thermodynamic Properties. *Inorg. Chem.* **2012**, *51*, 5427-5434.
6. Ma, E. S. F.; Mudalige, D. C.; James, B. R. Binding of CO and NH_3 at a five-coordinate Ru(II) centre in the solid state and in solution. *Dalton Trans.* **2013**, *42*, 13628-13634.
7. Ma, E. S. F.; Patrick, B. O.; James, B. R. Reactions of phenylacetylene and *p*-tolylacetylene with a five-coordinate Ru^{II} complex. *Inorg. Chim. Acta* **2013**, *408*, 126-130.
8. Ma, E. S. F.; Patrick, B. O.; James, B. R. Reversible binding of water, methanol, and ethanol to a five-coordinate ruthenium (II) complex. *Dalton Trans.* **2013**, *42*, 4291-4298.
9. da Silva, J. P.; Fagundes, F. D.; Back, D. F.; Ellena; J.; James, B. R.; de Araujo, M. P. Studies on the Ru(II) monocationic complexes $[RuCl_2)(NO)(P–N)(PPh_3)]PF_6$, where P–N = o-

diphenylphosphino-N,N-dimethylaniline, and R = Ph and *p*-X-C_6H_4 (X = OMe, Me, F). *Inorg. Chim. Acta* **2017**, *454*, 40-45.

10. Jessop, P. G.; Rettig, S. J.; Lee, C.-L.; James, B. R. Hydrido Thiolato and Thiolato Complexes of Ruthenium(II) Carbonyl phosphines. *Inorg. Chem.* **1991**, *30*, 4617-4627.
11. Queiroz, S. L.; Batista, A. A.; Oliva, G.; Gambardella, M. T. d. P.; Santos, R. H. A.; MacFarlane, K. S.; Rettig, S. J.; James, B. R. The reactivity of five-coordinate Ru(II) (1,4-bis(diphenylphosphino)butane) complexes with the N-donor ligands: ammonia, pyridine, 4-substituted pyridines, 2,2′-bipyridine, bis(*o*-pyridyl)amine, 1,10-phenanthroline, 4,7-diphenylphenanthroline and ethylenediamine. *Inorg. Chim. Acta* **1998**, *267*, 209-221.
12. MacFarlane, K. S.; Joshi, A. M.; Rettig, S. J.; James, B. R. Characterization of Five-Coordinate Ruthenium(II) Phosphine Complexes by X-ray Diffraction and Solid-State ^{31}P CP/MAS NMR Studies and Their Reactivity with Sulfoxides and Thioethers. *Inorg. Chem.* **1996**, *35*, 7304-7310.
13. Olivieri, A. A Correlation between P-31 NMR Chemical-Shift Tensors in Solid Phosphates and P-O Bond Lengths - Implications for Proton-Transfer Processes. *J. Mag. Res.* **1990**, *88*, 1-8.
14. Un, S.; Klein, M. P. Study of ^{31}P NMR Chemical Shift Tensors and Their Correlation to Molecular Structure. *J. Am. Chem. Soc.* **1989**, *111*, 5119-5124.
15. Ling, Y.; Zhang, Y. Deciphering the NMR Fingerprints of the Disordered System with Quantum Chemical Studies. *J. Phys. Chem. A* **2009**, *113*, 5993-5997.
16. Ortuño, M. A.; Castro, L.; Bühl, M. Computational Insight into ^{103}Rh Chemical Shift–Structure Correlations in Rhodium Bis(phosphine) Complexes. *Organometallics*, **2013**, *32*, 6437-6444.
17. Frisch, M. J.; Trucks, G. W.; Schlegel, H. B.; Scuseria, G. E.; Robb, M. A.; Cheeseman, J. R.; Scalmani, G.; Barone, V.; Mennucci, B.; Petersson, G. A.; Nakatsuji, H.; Caricato, M.; Li, X.; Hratchian, H. P.; Izmaylov, A. F.; Bloino, J.; Zheng, G.; Sonnenberg, J. L.; Hada, M.; Ehara, M.; Toyota, K.; Fukuda, R.; Hasegawa, J.; Ishida, M.; Nakajima, T.; Honda, Y.; Kitao, O.; Nakai, H; Vreven, T.; Montgomery, J. A.; Peralta, Jr. J. E.; Ogliaro, F.; Bearpark, M.; Heyd, J. J.; Brothers, E.; Kudin, K. N.; Staroverov, V. N.; Kobayashi, R.; Normand, J.; Raghavachari, K.; Rendell, A.; Burant, J. C.; Iyengar, S. S.; Tomasi, J.; Cossi, M.; Rega, N.; Millam, J. M.; Klene, M.; Knox, J. E.; Cross, J. B.; Bakken, V.; Adamo, C.; Jaramillo, J.; Gomperts, R.; Stratmann, R. E.; Yazyev, O.; Austin, A. J.; Cammi, R.; Pomelli, C.; Ochterski, J. W.; Martin, R. L.; Morokuma, K.; Zakrzewski, V. G.; Voth, G. A.; Salvador, P.; Dannenberg, J. J.; Dapprich, S.; Daniels, A. D.; Farkas, Ö.; Foresman, J. B.; Ortiz, J. V.; Cioslowski, J.; Fox, D. J. Gaussian 09 (Gaussian, Inc., Wallingford CT, 2009) Version D.01.
18. Adamo, C.; Barone, V. Toward reliable density functional methods without adjustable parameters: The PBE0 model. *J. Chem. Phys.* **1999,** *110*, 6158-6170.
19. Grimme, S.; Ehrlich S.; Goerigk, L. Effect of the Damping Function in Dispersion Corrected Density Functional Theory. *J. Comp. Chem*. **2011**, *32,* 1456-1465.

20. (a) Andrae, D.; Häussermann, U.; Dolg, M.; Stoll, H.; Preuss, H. Energy-adjustable *ab initio* pseudopotentials for the second and third row transition elements. *Theor. Chim. Acta* **1990**, *77*, 123-141. (b) Martin, J. M. L.; Sundermann, A. Correlation consistent valence basis sets for use with the Stuttgart–Dresden–Bonn relativistic effective core potentials: The atoms Ga–Kr and In–Xe. *J. Chem. Phys.* **2001**, *114*, 3408-3420.
21. Jensen, F. Unifying General and Segmented Contracted Basis Sets. Segmented Polarization Consistent Basis Sets. *J. Chem. Theory Comput.* **2014**, *10*, 1074-1085.
22. te Velde, G.; Bickelhaupt, F. M.; Baerends, E. J.; Fonseca Guerra, C.; van Gisbergen, S. J. A.; Snijders, J. G.; Ziegler, T. Chemistry with ADF. *J. Comp. Chem.* **2001**, *22*, 931-967. Amsterdam Density Functional (ADF) Theoretical Chemistry Vrieje Universitet see http://www.scm.com/ VERSION 2017.
23. (a) van Lenthe, E.; Baerends, E. J.; Snijders, J. G. Relativistic regular two-component Hamiltonians. *J. Chem. Phys.* **1993**, *99*, 4597. (b) van Lenthe, E.; Baerends, E. J.; Snijders, J. G. Relativistic total energy using regular approximations. *J. Chem. Phys.* **1994**, *101*, 9783-9792. (c) van Lenthe, E.; Baerends, E. J.; Snijders, J. G. Geometry optimizations in the zero-order regular approximation for relativistic effects. *J. Chem. Phys.* **1999**, *110*, 8943-8953. (d) van Lenthe, E.; Baerends, E. J.; Snijders, J. G. The zero-order regular approximation for relativistic effects: The effect of spin–orbit coupling in closed shell molecules. *J. Chem. Phys.* **1996**, *105*, 6505-6516. (e) van Lenthe, E.; van Leeuwen, R.; Baerends, E. J.; Snijders, J. G. Relativistic regular two-component Hamiltonians. *Int. J. Quant. Chem.* **1996**, *57*, 281-293.
24. Vícha, J.; Novotný, J.; Komorovsky, S.; Straka, M.; Kaupp, M.; Marek, R. Relativistic Heavy-Neigbor-Atom Effects on NMR Shifts: Concepts and Trends across the Periodic Table. *Chem. Rev*. **2020**, *120*, 7065-7103.
25. (a) Weinhold, F.; Landis, C. R. Valency and Bonding: A Natural Bond Orbital Donor-Acceptor Perspective. Cambridge University Press 2005. (b) Weinhold, F.; Landis, C. R. Discovering Chemistry with Natural Bond orbitals. Wiley 2012. (c) Glendening, E. D.; Badenhoop, J. K.; Reed, A. E.; Carpenter, J. E.; Bohmann, J. A.; Morales, C. M.; Landis, C. R.; Weinhold, F. Theoretical Chemistry Institute. University of Wisconsin. Madison. WI. USA 2013. http://nbo6.chem.wisc.edu/.
26. (a) Bohmann, J. A.; Weinhold, F.; Farrar, T. C. J. Natural chemical shielding analysis of nuclear magnetic resonance shielding tensors from gauge-including atomic orbital calculations. *J. Chem. Phys.* **1997**, *107*, 1173-1184. (b) Autschbach, J.; Zheng, T. Analyzing Pt chemical shifts calculated from relativistic density functional theory using localized orbitals: The role of Pt 5d lone pairs. *Magn. Reson. Chem.* **2008**, *46*, S45-S55. (c) Autschbach, J. Analyzing NMR shielding tensors calculated with two-component relativistic methods using spin-free localized molecular orbitals. *J. Chem. Phys.* **2008**, *128*, 164112. (d) Aquino, F.; Pritchard, B.; Autschbach, J. Scalar Relativistic Computations and Localized Orbital Analyses of Nuclear

Hyperfine Coupling and Paramagnetic NMR Chemical Shifts. *J. Chem. Theory Comp.* **2012**, *8*, 598-609.

27. Feindel, K. W.; Wasylishen, R. E. Phosphorus magnetic shielding tensors for transition-metal compounds containing phosphine, phosphido, and phosphinidene ligands: Insights from computational chemistry. *Can. J. Chem.* **2004**, *82*, 27-44.
28. Stoychev, G. L.; Auer, A. A.; Neese, F. Efficient and Accurate Prediction of Nuclear Magnetic Resonance Shielding Tensors with Double-Hybrid Density Functional Theory. *J. Chem. Theory Comp.* **2018**, *14*, 4756−4771.
29. Sun, M.; Zhang, I. Y.; Wu, A.; Xu, X. Accurate prediction of nuclear magnetic resonance shielding constants: towards the accuracy of CCSD(T) complete basis set limit. *J. Chem. Phys.* **2013**, *138*, 124113.
30. Teal, A. M.; Lutnæs, O. B.; Helgaker, T.; Tozer, D. J.; Gauss, J. Benchmarking density-functional theory calculations of NMR shielding constants and spin–rotation constants using accurate coupled-cluster calculations. *J. Chem. Phys.* **2013**, *138*, 024111.
31. Jameson, C. J. ; De Dios, A.; Jameson, A. K. Absolute Shielding Scale for ^{31}P from Gas phase NMR Studies. *Chem Phys. Lett.* **1990**, *167*, 575-582.
32. Lantto, P.; Jackowski, K.; Makulski, W.; Olejniczak, M.; Jaszunski, M. NMR Shielding Constants in PH_3. Absolute Shielding Scale. and the Nuclear Magnetic Moment of ^{31}P. *J. Phys. Chem. A.* **2011**, *115*, 10617-10623.
33. A complete search of isomers, carried out for $RuCl_2(P–N)(PR_3)(CO)$, found two *cis* isomers more stable than the observed *trans* complex. Only the most stable of the two *cis*-isomers, which further is topologically equivalent to the *cis* isomer found for all other L ligand is reported.
34. Tsipis, A. C. Building *trans*-philicity (*trans*-effect/*trans*-influence) ladders for octahedral complexes by using an NMR probe. *Dalton Trans.* **2019**, *48*, 1814-1822.
35. (a) Khoroshun, D. V.; Musaev, D. G.; Morokuma, K. Electronic reorganization: Origin of sigma trans promotion effect. *J. Comput. Chem.* **2007**, *28*, 423–441. (b) R. F.; Kozina. D. Quantification of the trans influence in d^8 square planar and d^6 octahedral complexes: a database study. *J. Coord. Chem.* **2013**, *66*, 490-500. (c) Pinter, B.; Van Speybroeck, V.; Waroquier, M.; Geerlings, P.; De Proft, F. *trans* effect and *trans* influence: importance of metal mediated ligand–ligand repulsion. *Phys. Chem. Chem. Phys.* **2013**, *15*, 17354-17365.
36. See for instance Caulton. K. G. The influence of π-stabilized unsaturation and filled-filled repulsions in transition metal chemistry. *New J. Chem.* **1994**, *18*, 25-41.
37. It is not easy to estimate the relative π-accepting ability of H_2 relative to ligands like NO^+, N_2O and N_2 but it is probably the weakest of them. For a review on the challenge to reproduce the coordination of H_2 by computations see Maseras. F.; Lledós. A.; Clot. E.; Eisenstein. O. Transition Metal Polyhydrides. From Qualitative ideas to Reliable Computational Studies. *Chem. Rev.* **2000**, *100*, 601-636.

38. (a) Moellmann, J.; Grimme, S. Influence of Crystal Packing on an Organometallic Ruthenium(IV) Complex Structure: The Right Distance for the Right Reason. *Organometallics* **2013**, *32*, 3784-3787. (b) Jacobsen, H. Its Environment Engraves the Geometry of a Molecular Entity: Allyl Coordination within a Dicationic Ruthenium(IV) Complex. *Organometallics* **2017**, *36*, 1770-1775. (c) Grimme, S.; Steinmetz, M. Effects of London dispersion correction in density functional theory on the structures of organic molecules in the gas phase. *Phys. Chem. Chem. Phys.* **2013**, *15,* 16031-16042.
39. Castro, A. C.; Fliegl, H., Cascella, M.; Helgaker, T.; Repisky, M.; Komorovsky, S.; Medrano, M. A.; Quiroga, A. G.; Swart. M. Four-component relativistic ^{31}P NMR calculations for trans-platinum(II) complexes: importance of the solvent and dynamics in spectral simulations. *Dalton Trans.* **2019**, *48*, 8076-8083.
40. It should be pointed out that large value of occupancy of an empty orbital usually indicates that the valence-bond structure of the complex is better represented with a covalent Ru-L bond than a Ru–P_A bond but the analysis presented in this work requires that the same Lewis structure is used for all complexes. In addition, the NBO analysis appears to be acceptable even for high value of $n\sigma^*$(Ru–P_A).
41. Viesser, R. N.; Ducati, L. C.; Tormena, C. F.; Autschbach, J. The unexpected roles of σ and π orbitals in electron donor and acceptor group effects on the ^{13}C NMR chemical shifts in substituted benzenes. *Chem. Sci.* **2017**, *8*, 6570-6576.
42. Halbert, S.; Copéret, C.; Raynaud, C.; O. Eisenstein, O. Elucidating the Link between NMR Chemical Shifts and Electronic Structure in d^0 Olefin Metathesis Catalysts. *J. Am. Chem. Soc.* **2016**, *138*, 2261-2272.
43. Yamamoto, K.; Gordon, C. P.; Liao, W.-C.; Copéret, C.; Raynaud, C. Eisenstein, O. Orbital Analysis of Carbon-13 Chemical Shift Tensors Reveals Patterns to Distinguish Fischer and Schrock Carbenes. *Angew. Chem. Int. Ed.* **2017**, *56*, 10127-10131.
44. Facelli, J. C. Chemical shift tensors: Theory and application to molecular structural problems. *Prog. Nucl. Magn. Reson. Spectrosc.* **2011**, *58*, 176−201.
45. Widdifield, C. M.; Schurko, R. W. Understanding Chemical Shielding Tensors Using Group Theory, MO Analysis, and Modern Density-Functional Theory. *Concepts Magn. Reson.* Part A **2009**, *34A*, 91-123.
46. Bühl, M.; Kaupp, M.; Malkina, O. L.; Malkin, V. G. The DFT route to NMR chemical shifts. *J. Comput. Chem.* **1999**, *20*, 91−105.
47. Kaupp, M. Interpretation of NMR Chemical Shifts. In *Calculation of NMR and EPR Parameters*; Kaupp, M., Bühl, M., Malkin, V. G., Eds.; Wiley-VCH: Weinheim, **2004**; pp 293−306.
48. Falivene, L.; Cavallo, L. Theoretical NMR spectroscopy of N-heterocyclic carbenes and their metal complexes. *Coord. Chem. Rev.* **2017**, *344*, 101-114.

49. Haller, L. J. L.; Mas-Marza, E.; Cybulski, M. K.; Sanguramath, R. A.; Macgregor, S. A.; Mahon, M. F.; Raynaud, C.; Russel, C. A.; Whittlesey, M. K. Computation provides chemical insight into the diverse hydride NMR chemical shifts of $[Ru(NHC)_4(L)H]^{(0/+)}$ species (NHC = N-heterocyclic carbene; L = vacant, H_2, N_2, CO, MeCN, O_2, P_4, SO_2, H^-, F^- and Cl^-) and their $[Ru(R_2PCH_2CH_2PR_2)_2(L)H]^{(+)}$ congeners. *Dalton Trans.* **2017**, 46, 2861-2873.
50. Gordon, C. P.; Yamamoto, K.; Liao, W.-C.; Allouche, F.; Andersen, R. A.; Copéret, C.; Raynaud, C.; Eisenstein, O. Metathesis Activity Encoded in the Metallacyclobutane Carbon-13 NMR Chemical Shift Tensors. *ACS Cent. Sci.* **2017**, *3*, 759−768.
51. Marchione, D.; Izquierdo, M. A.; Bistoni, G.; Havenith R. W. A.; Macchioni, A.; Zuccaccia, D.; Tarantelli, F.; Belpassi, L. C-13 NMR Spectroscopy of N-Heterocyclic Carbenes Can Selectively Probe sigma Donation in Gold(I) Complexes. *Chem. Eur-J.* **2017**, *23*, 2722-2778.
52. Gordon, C. P.; Shirase, S.; Yamamoto, K.; Andersen, R. A.; Eisenstein, O.; Copéret, C. NMR chemical shift analysis decodes olefin oligo- and polymerization activity of d^0 group 4 metal complexes. *Proc. Nat. Acad. Science* **2018**, 115, E5867-E5876.
53. Gordon, C. P.; Yamamoto, K.; Searles, K.; Shirase, S.; Andersen, R. A.; Eisenstein, O.; Copéret, C. Metal alkyls programmed to generate metal alkylidenes by α-H abstraction: prognosis from NMR chemical shift. *Chem. Sci.,* **2018**, *9*, 1912–1918.
54. Gordon, C. P.; Culver, D.; Conley, M.; Eisenstein, O.; Andersen, R. A.; Copéret, C. π-Bond Character in Metal–Alkyl Compounds for C–H Activation: How, When, and Why? *J. Amer. Chem. Soc.* **2018**, *141*, 648-656.
55. Gordon, C. P.; Raynaud, C.; Andersen, R; A.; Copéret, C.; Eisenstein, O. Carbon-13 NMR Chemical Shift: A Descriptor for Electronic Structure and Reactivity of Organometallic Compounds. *Acc. Chem. Res.* **2019**, *52*, 2278-2289.
56. (a) Zilm, K. W.; Conlin, R. T.; Grant, D. M.; Michl, J. Low-temperature natural-abundance Carbon-13 NMR spectroscopy of matrix-isolated Species. The anisotropy of the shielding tensor in ethylene. *J. Am. Chem. Soc.* **1978**, *100*, 8038−8039. (b) Arduengo, A. J.; Dixon, D. A.; Kumashiro, K. K.; Lee, C.; Power, W. P.; Zilm, K. W. Chemical Shielding Tensor of a Carbene. *J. Am. Chem. Soc.* **1994**, *116*, 6361−6367. (c) Wiberg, K. B.; Hammer, J. D.; Keith, T. A.; Zilm, K. NMR Chemical Shifts. 2. Interpretation of the Carbon Chemical Shifts in Monocyclic Aromatic Compounds and Carbenes. *J. Phys. Chem. A* **1999**, *103*, 21−27. (d) Wiberg, K. B.; Hammer, J. D.; Zilm, K. W.; Cheeseman, J. R. NMR Chemical Shifts. 3. A Comparison of Acetylene, Allene, and the Higher Cumulenes. *J. Org. Chem.* **1999**, *64*, 6394−6400.
57. (a) Azofra, L. M; Veenboer, R. M. P.; Falivene, L.; Vummaleti, S. V. C.; Poater, A.; Nolan, S. P.; Cavallo, L. Quantifying electronic similarities between NHC-gold(I) complexes and their isolobal imidazolium precursors. *Phys. Chem. Chem. Phys.* **2019**, *21*, 15615-15622. (b) Izquierdo, M. A.; Tarantelli, F.; Broer, R.; Bistoni, G.; Belpassi, L.; Havenith, R. W. A.

Orbital Decomposition of the Carbon Chemical Shielding Tensor in Gold(I) N-Heterocyclic Carbene Complexes. *Eur. J. Inorg. Chem.* **2020**, 1177-1183.

58. (a) Cavalieri, J. D.; West, R.; Duchamp, J. C.; Zilm, K. W. Unusual Silicon-29 Chemical-Shift Anisotropies in Three-Membered Rings. *J. Am. Chem. Soc.* **1993**, *115*, 3770−3771. (b) West, R.; Cavalieri, J. D.; Buffy, J. J.; Fry, C.; Zilm, K. W.; Duchamp, J. C.; Kira, M.; Iwamoto, T.; Müller, T.; Apeloig, Y. A Solid-State ^{1}NMR and Theoretical Study of the Chemical Bonding in Disilenes. *J. Am. Chem. Soc.* **1997**, *119*, 4972−4976. (c) Buffy, J. J.; West, R.; Bendikov, M.; Apeloig, Y. Chemical Shielding Tensors for a Silicon-Carbon Double Bond. *J. Am. Chem. Soc.* **2001**, *123*, 978−979. (d) Auer, D.; Strohmann, C.; Arbuznikov, A. V.; Kaupp, M.; Understanding Substituents Effects on ^{29}Si Chemical Shifts and Bonding in Disilenes. A Quantum Chemical Analysis. *Organometallics* **2003**, 22, *12*, 2442–2449. (e) Auer, D.; Kaupp, M.; Strohmann, C. "Unexpected" ^{29}Si NMR Chemical Shifts in Heteroatom-Substituted Silyllithium Compounds: A Quantum-Chemical Analysis. *Organometallics* **2004**, *23*, 3647-3655. (f) Kravchenko, V.; Kinjo, R.; Sekiguchi, A.; Ichinohe, M.; West, R.; Balazs, Y. S.; Schmidt, A.; Karni, M.; Apeloig, Y. Solid-State ^{29}Si NMR Study of RSiSIR: A Tool for Analyzing the Nature of the Si-Si Bond. *J. Am. Chem. Soc.* **2006**, *128*, 14472–14473. (g) Epping, J. D.; Yao, S.; Karni, M.; Apeloig, Y.; Driess, M. Si=X Multiple Bonding with Four-Coordinate Silicon? Insights into the Si=O and Si=S Double Bonds in Stable Silanoic Esters and Related Thioesters: A Combined NMR Spectroscopic and Computational Study. *J. Am. Chem. Soc.* **2010**, *132*, 5443-5445.
59. Lam, E.; Copéret, C. Understanding Trends in Al-27 Chemical Shifts and Quadrupolar Coupling Constants in Chloroalkyl Aluminum $[AlCl_x(Me)_{(3-x)}]_{(n = 1 \text{ or } 2)}$ Compounds. *Helv. Chim. Acta* **2018**, *101*, e1800120
60. Lätsch, L.; Lam, E; Copéret, C. Electronegativity and location of anionic ligands drive yttrium NMR for molecular, surface and solid-state Structures. *Chem. Sci.* **2020**, *11,* 6724-6735.
61. Ehinger, C.; Gordon, C. P.; Copéret, C. Oxygen transfer in electrophilic epoxidation probed by O-17 NMR: differentiating between oxidants and role of spectator metal oxo. *Chem. Sci.* **2019**, *10*, 1786-1795.
62. Pietrasiak, E.; Gordon, C. P.; Copéret, C.; Togni, A. Understanding Te-125 NMR chemical shifts in disymmetric organo-telluride compounds from natural chemical shift analysis. *Phys. Chem. Chem. Phys.* **2020**, *22*, 2319-2326.
63. Vummaleti, S. V. C.; Nelson, D. J.; Poater, A.; Gómez-Suárez, A.; Cordes, D. B.; Slawin, A. M. Z.; Nolan, S. P.; Cavallo, L. What can NMR spectroscopy of selenoureas and phosphinidenes teach us about the π-accepting abilities of *N*-heterocyclic carbenes? *Chem. Sci.* **2015**, *6*, 1895-1904

64. Duchamp, J. C.; Pakulski, M.; Cowley, A. H.; Zilm, K. W. Nature of the carbon-phosphorus double Bond and the carbon-phosphorus triple bond as studied by solid-state NMR. *J. Am. Chem. Soc.* **1990**, *112*, 6803−6809.
65. Wu, G.; Rovnyak, D.; Johnson, M. J. A.; Zanetti, N. C.; Musaev, D. G.; Morokuma, K.; Schrock, R. R.; Griffin, R. G.; Cummins, C. C. Unusual ^{31}P Chemical Shielding Tensors in Terminal Phosphido Complexes Containing a Phosphorus-Metal Triple Bond. *J. Am. Chem. Soc.* **1996**, *118*, 10654−10655.
66. (a) Eichele, K.; Wasylishen, R. E.; Corrigan, J. F. Talor, N. J.; Carty, A. J. Phosphorus-31 chemical shift tensors of phosphinidene ligands in ruthenium carbonyl clusters: a ^{31}P single-crystal and CP/MAS-NMR study. *J. Am. Chem. Soc.* **1995**, *117*, 6961-6969. (b) Eichele, K.; Wasylishen, R. E.; Corrigan, J. F.; Taylor, N. J.; Carty, A. J.; Feindel, K. W.; Bernard, G. M. Phosphorus Chemical Shift Tensors of Phosphido Ligands in Ruthenium Carbonyl Compounds: ^{31}P NMR Spectroscopy of Single-Crystal and Powder Samples, and ab Initio Calculations. *J. Am. Chem. Soc.* **2002**, *124*, 1541-1552.
67. Feindel, K. W.; Wasylishen, R. E. Phosphorus magnetic shielding tensors for transition-metal compounds containing phosphine, phosphido, and phosphinidene ligands: Insights from computational chemistry. *Can. J. Chem.* **2004**, *82*, 27-44.
68. Bernard, G. M.; Feindel, K. W.; Wasylishen, R. E.; Cameron, T. S. Solid-state phosphorus-31 NMR spectroscopy of a multiple-spin system: an investigation of a rhodium-triphosphine complex. *Phys. Chem. Chem. Phys.* **2008**, *10*, 5552-5563.
69. The partition into diamagnetic and paramagnetic terms has no physical meanings as these terms can be rebalanced by changing the gauge origin. However, within a given choice of gauge origin, the relative variations of these two terms and their respective per-MO contributions are representative of a given species and thus meaningful to chemists.
70. The spin orbit term is small and while it improves the quality of the calculations it does not determine the trends as a function of L. For this reason, only the paramagnetic contribution is discussed.
71. Jameson, C. J.; Gutowsky, H. S. Calculation of Chemical Shifts. I. General Formula and Z Dependence. *J. Chem. Phys.* **1964**. *40*, 1714-1724.
72. Sutter, K.; Autschbach, J. Computational Study and Molecular Orbital Analysis of NMR Shielding, Spin-Spin Coupling, and Electric Field Gradients of Azido Platinum Complexes. *J. Am. Chem. Soc.* **2012**, *134*, 13374-13385.

TABLE OF CONTENT GRAPHIC and SYNOPSIS

The experimental correlation established between Ru–P distances and ^{31}P NMR chemical shifts in $RuCl_2(P–N)(PR_3)L$ (L = none, H_2O, H_2S, CH_3SH, H_2, N_2, N_2O, NO^+, C=CHPh, and CO; P–N = o-diphenylphosphino-N,N'-dimethylaniline) is well reproduced with DFT calculations and, through a study of the *P* chemical shift tensors and the paramagnetic contributions to the shielding, shown to be mostly associated with the σ-donor strength of the L ligands.